Earth and Planetary Science Letters 450 (2016) 243–253

Contents lists available at ScienceDirect

Earth and Planetary Science Letters

www.elsevier.com/locate/epsl

Evaluation of siderite and magnetite formation in BIFs by pressure–temperature experiments of Fe(III) minerals and microbial biomass

Maximilian Halama [a], Elizabeth D. Swanner [b], Kurt O. Konhauser [c], Andreas Kappler [a,*]

[a] Geomicrobiology, Center for Applied Geosciences, University of Tuebingen, Tuebingen, Germany
[b] Department of Geological and Atmospheric Sciences, Iowa State University, Ames, IA 50011, USA
[c] Department of Earth and Atmospheric Sciences, University of Alberta, Edmonton, Alberta, T6G 2E3, Canada

ARTICLE INFO

Article history:
Received 22 February 2016
Received in revised form 12 June 2016
Accepted 18 June 2016
Available online xxxx
Editor: D. Vance

Keywords:
banded iron formations
metamorphic
Fe(III) reduction
mineralogy

ABSTRACT

Anoxygenic phototrophic Fe(II)-oxidizing bacteria potentially contributed to the deposition of Archean banded iron formations (BIFs), before the evolution of cyanobacterially-generated molecular oxygen (O_2), by using sunlight to oxidize aqueous Fe(II) and precipitate Fe(III) (oxyhydr)oxides. Once deposited at the seafloor, diagenetic reduction of the Fe(III) (oxyhydr)oxides by heterotrophic bacteria produced secondary Fe(II)-bearing minerals, such as siderite ($FeCO_3$) and magnetite (Fe_3O_4), via the oxidation of microbial organic carbon (i.e., cellular biomass). During deeper burial at temperatures above the threshold for life, thermochemical Fe(III) reduction has the potential to form BIF-like minerals. However, the role of thermochemical Fe(III) reduction of primary BIF minerals during metamorphism, and its impact on mineralogy and geochemical signatures in BIFs, is poorly understood. Consequently, we simulated the metamorphism of the precursor and diagenetic iron-rich minerals (ferrihydrite, goethite, hematite) at low-grade metamorphic conditions (170 °C, 1.2 kbar) for 14 days by using (1) mixtures of abiotically synthesized Fe(III) minerals and either microbial biomass or glucose as a proxy for biomass, and (2) using biogenic minerals formed by phototrophic Fe(II)-oxidizing bacteria. Mössbauer spectroscopy and μXRD showed that thermochemical magnetite formation was limited to samples containing ferrihydrite and glucose, or goethite and glucose. No magnetite was formed from Fe(III) minerals when microbial biomass was present as the carbon and electron sources for thermochemical Fe(III) reduction. This could be due to biomass-derived organic molecules binding to the mineral surfaces and preventing solid-state conversion to magnetite. Mössbauer spectroscopy revealed siderite contents of up to 17% after only 14 days of incubation at elevated temperature and pressure for all samples with synthetic Fe(III) minerals and biomass, whereas 6% of the initial Fe(III) was reduced to sideritic Fe(II) in biogenic Fe(III) minerals during incubation. Based on our data, magnetite in BIF is unlikely to be formed by thermochemical Fe(III) reduction in sediments of biogenic ferrihydrite, hematite or goethite-dominated sediments with complex microbial biomass present. Instead, our results suggest that diagenetic magnetite in BIF was either formed by microbial Fe(III) reduction during early diagenesis, i.e., below 120 °C, or by thermochemical Fe(III) reduction with simple organic compounds at higher temperatures, whereas siderite was formed by both microbial, diagenetic Fe(III) reduction and thermogenic Fe(III) reduction with complex biomass. Thermochemical Fe(III) reduction coupled to biomass oxidation during metamorphism provides another origin for BIF siderites and could have led to a significant increase in Fe(II) content in BIF after deposition over geological timescales.

1. Introduction

1.1. Geochemical conditions and processes involved in banded iron formation deposition

Banded iron formations (BIFs) are Fe- and Si-rich sedimentary rocks deposited from the Eoarchean to the Paleoproterozoic, 3.8 to

* Corresponding author at: Geomicrobiology, Center for Applied Geosciences University of Tuebingen, Sigwartstrasse 10, D-72076 Tuebingen, Germany. Tel.: +49 7071 2974992; fax: +49 7071 29 295059.
E-mail address: andreas.kappler@uni-tuebingen.de (A. Kappler).

http://dx.doi.org/10.1016/j.epsl.2016.06.032
0012-821X/

1.7 billion years (Ga) ago. They are characterized by alternating Fe- and Si-rich layers with low organic carbon (C_{org}) (<0.2 wt.%) (see Bekker et al., 2010; 2014 for reviews). Silicon dioxide (SiO_2), up to 56 wt.% in BIFs, is mainly present in chert, but is also present in various iron silicate minerals. The BIF total iron content can be up to 40 wt.% and Fe is present as silicates, oxides (hematite, magnetite), carbonates (siderite, ankerite) and, to a minor extent, sulfides (pyrite) (Klein, 2005).

The current mineralogy of BIF is likely not primary, but instead represents post-depositional processes such as diagenesis (which we consider as biologically-driven and below 120 °C) and metamorphism (which occurs abiogenically at higher temperatures) (Klein, 2005; Konhauser et al., 2005; Li et al., 2011, 2013; Köhler et al., 2013; Posth et al., 2013; Rasmussen et al., 2014). The Si-rich layers in BIFs originated from the chemical precipitation of amorphous silica since Precambrian oceans were quite likely enriched in Si up to 2.2 mM (Siever, 1992; Konhauser et al., 2007b). For the Fe-rich layers, it is still debated which minerals formed the primary Fe-rich sediments (Klein, 2005; Rasmussen et al., 2014; Sun et al., 2015). The deposition of Fe-rich sedimentary precipitates requires certain geochemical conditions and processes to have occurred in the Archean and Paleoproterozoic ocean: (1) Since Fe(III) is poorly soluble in seawater at circumneutral pH, the ancient oceans must have been anoxic to transport a significant amount of Fe as dissolved Fe(II) to BIF deposition sites. (2) An oxidative process must have occurred in seawater that oxidized the dissolved Fe(II) to Fe(III), forming Fe(III) precipitates (Cornell and Schwertmann, 2003). The most widely assumed primary minerals are Fe(III) (oxyhydr)oxides, for instance, ferrihydrite, $Fe(OH)_3$. Ferrihydrite forms either by direct microbial oxidation via anoxygenic phototrophic Fe(II) oxidation (Konhauser et al., 2002; Kappler et al., 2005), indirectly by abiotic oxidation via free O_2 produced photosynthetically by cyanobacteria (Cloud, 1965), or by microaerophilic Fe(II)-oxidizing bacteria also using cyanobacterial O_2 (Holm, 1989). Additionally, photochemical oxidation of aqueous Fe(II) has been suggested as an abiotic origin for BIF (Braterman et al., 1983), but this process was likely inefficient compared to other oxidative mechanisms and simple precipitation from supersaturated solutions (Konhauser et al., 2007a). The deposited ferrihydrite then dehydrates under elevated pressure and/or temperature and is transformed to hematite (at $T < 100$ °C; Schwertmann et al., 1999), which is an abundant BIF mineral (Klein, 2005). In the presence of an electron donor, such as C_{org}, the ferrihydrite/hematite can also be reduced to mixed-valence or ferrous-iron-containing minerals, such as magnetite (Fe_3O_4) and siderite ($FeCO_3$) (Perry et al., 1973; Lovley et al., 1987; Johnson et al., 2005; Posth et al., 2013).

Although magnetite in BIF could be a primary phase that formed by interaction of Fe(III) (oxyhydr)oxide precipitates with dissolved Fe(II) during sedimentation to the seafloor (Hansel et al., 2003), both petrographic and isotopic evidence suggests magnetite is largely a secondary mineral phase (e.g., Ewers and Morris, 1981; Krapež et al., 2003). In terms of iron isotopes, light Fe isotope compositions in BIF magnetite are assumed to originate from dissimilatory Fe(III) reduction (DIR) (Johnson et al., 2005, 2008; Percak-Dennett et al., 2011). Furthermore, the oxidation of C_{org} during DIR would not only have diminished C_{org} in BIF sediments (e.g., Gole and Klein, 1981), but the isotopically depleted bicarbonate generated would have formed calcium carbonate cements with the isotopically depleted ^{13}C values that are characteristic of BIFs (Perry et al., 1973; Walker, 1984). Therefore, the presence of magnetite would indicate the original presence of C_{org} in BIF primary sediments and, consequently, the simultaneous deposition of Fe(III) minerals and biomass in Precambrian oceans (Li et al., 2011). Consequently, for BIF formed in the Eoarchean (4.0–3.6 Ga) and Paleoarchean (3.6–3.2 Ga), times for which there is at present no indication that cyanobacteria had yet evolved (see Satkoski et al., 2015 that recently argued for cyanobacteria at 3.2 Ga), the presence of Fe(III)-containing minerals would seemingly imply that phototrophic Fe(II)-oxidizing bacteria had already evolved (e.g., Pecoits et al., 2015). However, it needs to be considered that the absence of convincing evidence for cyanobacteria at that time does not exclude the possibility that cyanobacteria had already evolved.

Siderite is another ferrous-iron-containing mineral that is found in BIFs of all ages. Since Mesoarchean to Paleoproterozoic seawater had high concentrations of Fe(II) and higher HCO_3^- concentrations than today (due to a higher pCO_2 in the Precambrian atmosphere; Holland et al., 1986) it has been suggested that some siderite precipitated directly from seawater (Ewers and Morris, 1981; Pecoits et al., 2009). However, the carbon isotope composition of BIF siderite reveals enrichments of the light carbon isotope (^{12}C) with respect to seawater-derived inorganic carbon, suggesting that ^{12}C-enriched biomass carbon was mineralized by DIR and incorporated into Fe(II) carbonates (Beukes et al., 1990; Vargas et al., 1998; Konhauser et al., 2005).

1.2. Thermochemical origin of magnetite and siderite in BIFs – role of abiotic metamorphism

Any model describing the mechanisms by which secondary BIF minerals precipitated must also consider the possibility that the Fe(II) necessary for the formation of these two minerals was derived abiotically from Fe(III) in the presence of C_{org}, induced by elevated pressure and temperature conditions associated with sediment burial (Perry et al., 1973). Recent studies using P/T-burial simulations of synthetic mixtures of ferrihydrite, with glucose as a proxy for biomass, have demonstrated that magnetite and siderite can be formed by thermochemical Fe(III) reduction under low P/T metamorphic conditions (Köhler et al., 2013; Posth et al., 2013). In these experiments, ferrihydrite was mixed with glucose and then exposed to 1.2 kbar and 170 °C for up to 137 days, conditions comparable to those experienced by some of the best preserved BIF in South Africa and Western Australia (Klein, 2005). In the Posth et al. (2013) and Köhler et al. (2013) studies, the main Fe redox and mineral transformation took place within the first 14 days and the secondary mineral phases formed included various mixtures of hematite, magnetite and siderite, depending upon the amount of glucose initially added. Up to 23% of the initial Fe(III) in ferrihydrite was reduced to Fe(II). From that study it was concluded that thermochemical Fe(III) reduction could have contributed to siderite and magnetite formation in BIF. However, it is unknown what effect real microbial biomass (versus glucose) has in thermochemical transformations.

In the present study, we expanded the experiments by Posth et al. (2013) and Köhler et al. (2013) and simulated BIF metamorphism using two types of microbial biomass (dried microbial cells and temperature pre-treated microbial cells). Additionally, we conducted experiments with hematite and goethite as alternative Fe(III) sources to investigate the influence of the starting minerals on the resulting mineralogy. Hematite, a dehydration product of Fe(III) (oxyhydr)oxides (Cornell and Schwertmann, 2003), and goethite, a possible product of chemical oxidation under conditions proposed for Eoarchean to Paleoproterozoic oceans (Cornell and Schwertmann, 2003; Hansel et al., 2003) and of microbial Fe(II) oxidation (Kappler and Newman, 2004), represent alternative primary BIF minerals. However, synthetic minerals have different properties than biogenic minerals. Therefore, we ran additional experiments with biogenic Fe(III) mineral–cell aggregates, which were produced by phototrophic Fe(II)-oxidizing bacteria. Finally, we investigated the influence of Si sorbed to biogenic Fe(III) minerals on the thermochemical Fe(III) reduction, given the siliceous nature of Precambrian seawater, using biogenic Fe(III) mineral–

cell aggregates grown in the presence of approx. 1 mM Si in the medium. The ultimate goal of this study is to determine whether magnetite and siderite can be formed by thermochemical reduction of Fe(III) minerals by biomass in BIF relevant mixtures during metamorphic conditions.

2. Methods

2.1. Fe(III) mineral synthesis

Ferrihydrite, hematite, and goethite syntheses were performed according to Schwertmann and Cornell (2008) (SI. 1). All Fe(III) minerals were washed four times with Millipore water and freeze-dried. The identity and crystallinity were verified using µXRD and Mössbauer spectroscopy.

2.2. Microbial biomass synthesis

Microbial biomass was obtained by cultivation of *Shewanella oneidensis* MR-1 (modified after Lies et al., 2005), and the cells were washed and freeze-dried (SI. 2). The dried biomass was split in two fractions: the first remained untreated while the second was transferred into 15 cm-long glass tubes that were closed by welding for thermal decomposition treatments. The aim of this treatment was to partially decompose the biomass so that the temperature-treated (T-treated) biomass was depleted in highly reactive organic compounds like sugars and proteins (SI. 3). The glass tubes, filled with approximately 1 g biomass, were closed in a glove-box (100% N_2) with butyl stoppers. The glass tubes were welded by a gas torch after evacuation with a vacuum pump to avoid bursting. The closed glass tubes were incubated at 170 °C for 24 h. The T-treated biomass was homogenized by grinding after incubation.

2.3. Production of biogenic Fe(III) mineral–cell aggregates with and without sorbed Si

For production of biogenic Fe(III) mineral–cell aggregates, with and without Si, the marine phototrophic Fe(II)-oxidizing strain *Rhodovolum iodosum* was cultivated following Wu et al. (2014) (SI. 4). After complete Fe(II) oxidation, the Fe(III) mineral–cell aggregate suspension was centrifuged at 4229 g, the supernatant was discarded and the aggregates were washed four times with a marine phototroph medium diluted 1:10 with water. The aggregates were freeze-dried and the total organic carbon (TOC) content was quantified by an elemental analyzer (Elementar Vario EL). The Fe content was determined by the ferrozine assay (Stookey, 1970) after dissolution of an aliquot of the aggregates in 1 M HCl. The Si content of the Fe(III) mineral–cell aggregates precipitated in 1 mM dissolved Si was determined after dissolving the aggregates in HNO_3 using microwave plasma-atomic emission spectroscopy (MP-AES).

2.4. Capsule preparation

Mixtures of synthetic Fe(III) minerals and C_{org} sources (glucose/dried microbial biomass/T-treated dried microbial biomass) were prepared at electron ratios of 0.6 and 2.4: electrons that can be released from carbon vs. electrons that can be accepted by Fe(III). For further information regarding the calculation of the electron ratios see Posth et al. (2013). The electron ratio of 0.6 (corresponding to an excess of Fe(III); hereafter referred to as low C_{org} content) is comparable to the C:Fe ratio in sediments which are produced by phototrophic Fe(II)-oxidizing bacteria (Posth et al., 2010), whereas the electron ratio of 2.4 (corresponding to an excess of biomass; hereafter referred to as high C_{org} content) represents the additional input of C_{org} (e.g. organic matter from cyanobacteria). The electron ratios are used following previous studies by Köhler et al. (2013) and Posth et al. (2013).

The gold capsules (diameter 2.1 mm, 0.2 mm wall thickness, 3 cm long) were loaded with Fe(III) mineral–C_{org} mixtures and Fe(III) mineral–cell aggregates, welded in air and put in a high pressure/high temperature autoclave (SITEC SIEBER Engineering AG) at 170 °C and 1.2 kbar for 14 days (SI. 5). The sealing of the capsules was monitored by weighing before and after simulated metamorphism. As a non-treated control, a capsule containing ferrihydrite with high glucose content was prepared and not incubated at high temperature and pressure.

2.5. µXRD measurements

The gold capsules were opened and dried at 30 °C for 24 h in an incubator in a glove-box with 100% N_2. The sample material was picked from the gold capsules and ground. A small aliquot was put on a silicon wafer and stored in N_2-filled preserving jars until µXRD analyses under ambient atmospheric conditions (within a few minutes to avoid oxidation of O_2-sensitive Fe minerals).

A Bruker D8 Discover GADDS XRD^2-microdiffractometer from the Applied Mineralogy group at the University of Tübingen was used for µXRD equipped with a Co-anode, a primary graphite monochromator, and a 2-dimensional HI-STAR-detector. Crystalline minerals were identified by using the internal database of the EVA software (version 10.0.1.0).

2.6. Mössbauer spectroscopy

Samples were filled under N_2 in Plexiglas holders with an inner-diameter of 1.5 cm and spread evenly in the holders to form a thin disc. The samples were inserted into a closed-cycle exchange gas cryostat (Janis cryogenics). The spectra were recorded at 140 K for Fe(III) mineral–C_{org} mixtures and at room temperature (295 K, RT), 140 K, 77 K, and 5 K for pure minerals in transmission geometry using a constant acceleration drive system (WissEL). A ^{57}Co source embedded in a Rhodium matrix was used as gamma radiation source. The sample spectra were calibrated against a 7-µm-thick α-^{57}Fe foil at RT. The RECOIL software suite (University of Ottawa, Canada) was used for the calibration and spectra modeling using Voigt-based line shapes. The Lorentz half-width-half-maximum value was kept constant at the line width determined from the minimum line width of the third and fourth peak of the calibration foil in the models, and the Gauss' sigma parameter was used to account for line broadening until the fitting was reasonable.

Mössbauer spectra were obtained on at least triplicates of each mixture at 140 K and each spectrum was fitted individually (SI. 10). The relative proportion of the areas covered by the doublets and sextets of the total area of the Mössbauer spectrum is equivalent to the relative abundance of Fe in a particular crystal lattice site to the total Fe. The relative Fe(II) content was calculated assuming ideal stoichiometry with 100% Fe(II) in siderite and 50% Fe(II) in the octahedral site of magnetite (resulting in a total Fe(II) content of 33% in magnetite). Fe(II) contents are given as mean values with their 1σ standard deviations.

2.7. Thick section preparation and reflected-light microscopy

For reflected-light microscopy, gold capsules were opened at both ends in a glove-box (95/5 N_2/H_2), placed in plastic rings and embedded in Araldit 2020 using a vacuum embedder. After hardening, the samples were sawn in half and polished with 1 µm grit. A Leica DM 2500 P was used with a 20× objective. For XAS measurements, gold capsules were embedded in Körapox 439 and

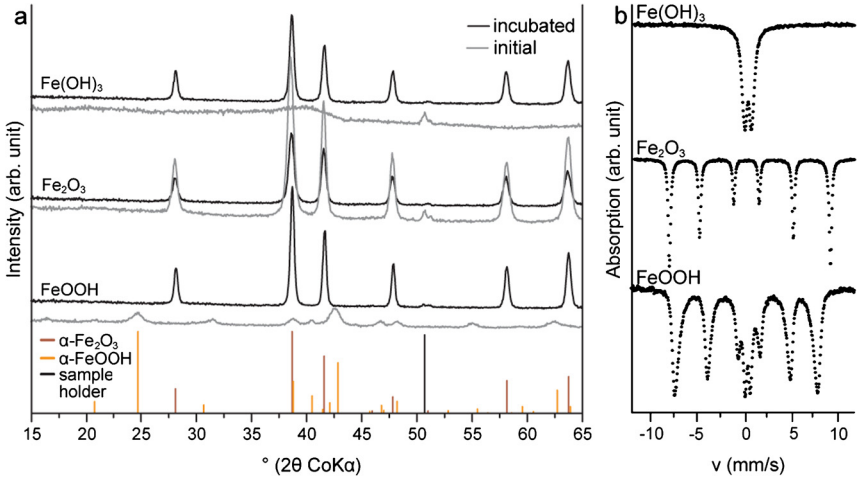

Fig. 1. X-ray diffractograms (a) of pure synthesized ferrihydrite, hematite, and goethite before and after incubation at 170 °C and 1.2 kbar for 14 days, and Mössbauer spectra (b) obtained at 77 K of the same pure mineral samples before incubation.

polished down until the sample was at the surface. Sample material was fixed with glue and further polished with 1 µm grit (SI. 6).

2.8. Synchrotron-based X-ray fluorescence and X-ray absorption spectroscopy

Synchrotron-based X-ray fluorescence (XRF) and X-ray spectroscopy (XAS) measurements of epoxy-mounted capsules around the Fe K-edge were made and analyzed as described in the Supplementary Information (SI. 7).

3. Results

3.1. Identity of minerals formed during simulated metamorphism of mixtures of synthetic Fe(III) minerals and C_{org}

For all starting minerals and experiments, the identified minerals and their Fe(II)/Fe(tot) ratios are shown in Table 1. The products of mineral syntheses were identified by µXRD and Mössbauer spectroscopy. Ferrihydrite synthesis produced poorly crystalline grains indicated by the absence of reflections in the X-ray diffractogram (Fig. 1a) and by the presence of a paramagnetic doublet in the Mössbauer spectrum, even at 77 K (Fig. 1b), indicating a low blocking temperature (SI. 8). The synthesis of pure hematite was confirmed by µXRD (as revealed by strong X-ray reflections, Fig. 1a) and a sextet in the Mössbauer spectrum showing magnetic ordering at 77 K and RT (Fig. 1b; SI. 9). Goethite was identified as poorly crystalline with probably small grain size by a paramagnetic component (goethite is usually characterized by a magnetic sextet even at room temperature; Cornell and Schwertmann, 2003) due to weak magnetic ordering in the Mössbauer spectrum at 77 K (Fig. 1b, SI. 10) and broad reflections with µXRD (Fig. 1a). Within 14 days of incubation at 170 °C and 1.2 kbar, the pure ferrihydrite and goethite (in the absence of C_{org}) were transformed completely to hematite, but the hematite was not altered (Fig. 1a).

When synthesized Fe(III) minerals were mixed with a source of C_{org}, the final mineralogy after pressure/temperature treatment was different depending on starting mineral identity, C_{org} identity and amount. Samples containing synthetic ferrihydrite and glucose, both with low and high C_{org} content, formed magnetite and siderite during incubation at 1.2 kbar and 170 °C for 14 days. In the ferrihydrite/glucose mixture with low C_{org} content, hematite formed as well (Fig. 2a). When glucose was substituted by either dried microbial biomass or by T-treated biomass, magnetite did not form in either low or high C_{org} content samples. Instead, only hematite and siderite were formed (Fig. 2a). When hematite was mixed with either glucose or cells (independent of low or high C_{org} content), siderite was produced (Fig. 2b). In contrast to ferrihydrite/glucose mixtures, no magnetite was formed if hematite was blended with glucose (Fig. 2b). When goethite was mixed with small amounts of glucose, magnetite formed (Fig. 2c; SI. 15). However, when the glucose content was increased, magnetite did not form from goethite during incubation (Fig. 2c). Instead, in all samples containing goethite and organics (dried or T-treated biomass or glucose), the formation of siderite was observed (Fig. 2c). The transformation of goethite to hematite was dependent on the C_{org} content and type of the C_{org} source. In goethite/glucose samples, no hematite formed (Fig. 2c). Similarly, hematite was not formed in the high C_{org}-containing goethite/dried biomass sample (Fig. 2c). Instead, reflections relating to maghemite, an Fe(III) oxide with magnetite structure and a known thermal transformation product of goethite in reducing environments (Cornell and Schwertmann, 2003; Hanesch et al., 2006), were detected (Fig. 2c). µXRD signals for hematite were present in the goethite samples with either high or low content of pre-treated biomass (Fig. 2c).

3.2. Identity of minerals formed during simulated metamorphism of biogenic Fe(III) mineral–cell aggregates

The starting mineralogy of biogenic Fe(III) mineral–cell aggregates from phototrophic Fe(II) oxidation was different depending on the presence or absence of Si. Fe(III) mineral–cell aggregates obtained from cultures of *R. iodosum* grown without Si consisted of poorly crystalline goethite, as indicated by very broad reflections in µXRD (Fig. 3a) and partly magnetic ordering at 77 K, expressed by the presence of a collapsed Mössbauer sextet (Fig. 3b; SI. 11). Aggregates produced in the presence of Si showed no reflections (Fig. 3a) and had a low blocking temperature revealed by the absence of any magnetic ordering at 77 K in the Mössbauer spectrum (Fig. 3b; SI. 12), characteristic for ferrihydrite. MP-AES showed that the Si content in biogenic Fe(III) mineral–cell aggregates formed by *R. iodosum* in the presence of 1 mM dissolved Si was about 1.4 wt.% and the Si/Fe ratio was 0.042. After incubation of the Fe(III) mineral–cell aggregates at 1.2 kbar and 170 °C for 14 days, µXRD analyses of samples, with and without Si, showed the presence of goethite, hematite and siderite (Fig. 3a). Additionally, in the setup with Si, a very weak signal for maghemite appeared (Fig. 3a). Both siderite and goethite were more abundant after incubation in the sample of biogenic Fe(III) mineral–cell aggregates without Si, as indicated by higher reflection intensities. Goethite was also

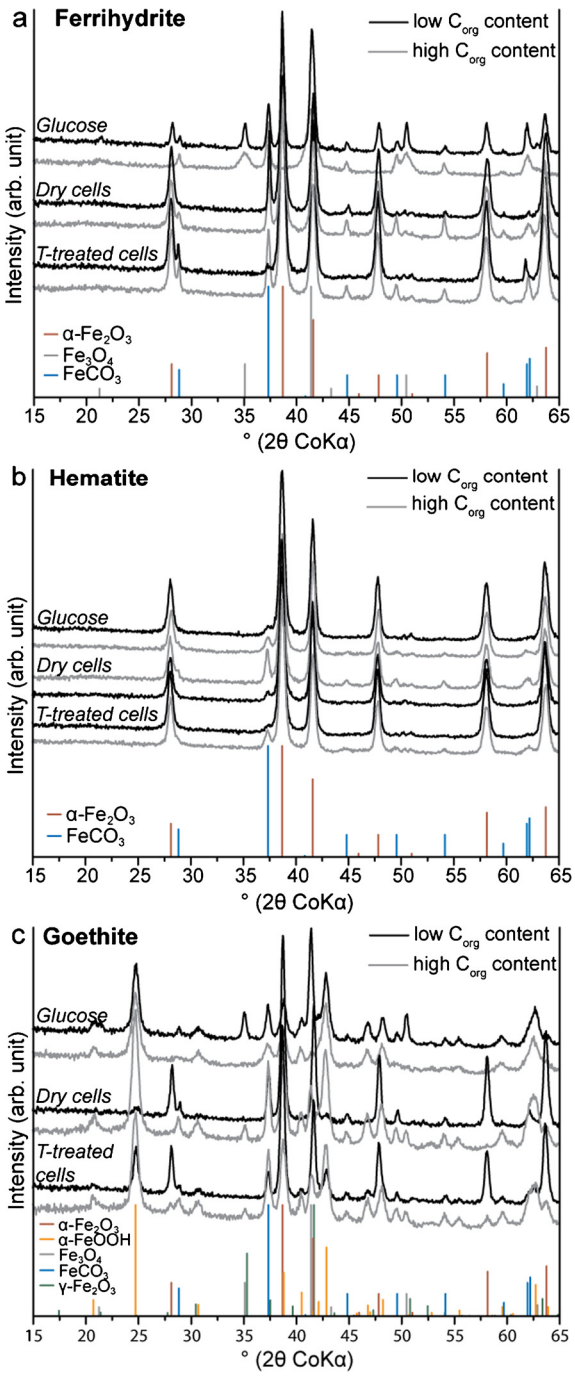

Fig. 2. µXRD analyses of samples containing ferrihydrite (a), hematite (b), and goethite (c) after simulated P/T-diagenetic incubation with high or low amounts of pre-treated and non-treated microbial biomass compared to setups incubated with glucose.

more crystalline, resulting in narrower reflections compared to reflections in the sample of biogenic Fe(III) mineral–cell aggregates with Si (Fig. 3a).

3.3. Calculation of Fe(II) and Fe(III) based on results from Mössbauer spectroscopy

Mössbauer spectroscopy was used to determine Fe(II)/Fe(tot) ratios and to complement the µXRD identification of the minerals in the P/T-diagenetic products of different Fe(III) mineral–C_{org} mixtures.

Our results showed that magnetite formation is limited to ferrihydrite/glucose (low and high content) and goethite/glucose (low content) samples (Table 1; SI. 13, 15). In contrast, siderite was found in all synthetic Fe(III) mineral-C_{org} mixtures, as well as in both biogenic setups (Table 1). Non-reduced initial ferrihydrite was completely transformed to hematite (Table 1; SI. 13) and non-reduced initial hematite remained stable during simulated metamorphism (Table 1; SI. 14). Goethite remained partially stable in all goethite setups, but the amount of remaining goethite depended on the C_{org} content (Table 1; SI. 15). In goethite/glucose (high content) samples no hematite formed (Table 1). In goethite setups with high contents of dried and T-treated biomass maghemite appeared as an additional phase (Table 1; SI. 15).

Fe(II) quantification showed that thermochemical Fe(III) reduction during simulated metamorphism of ferrihydrite/glucose mixtures with low and high C_{org} contents produced 22.8 ± 0.9% and 43.9 ± 1.6% Fe(II), respectively (Table 1). When glucose was substituted by dried microbial cells, the Fe(II) decreased to 4.7 ± 0.6% and 14.6 ± 0.3% in ferrihydrite/biomass mixtures with low and high C_{org} content, respectively (Table 1). The Fe(II) in samples containing ferrihydrite and T-pre-treated microbial biomass with low and high C_{org} was 3.3 ± 0.4% and 12.0 ± 1.2%, respectively (Table 1). The control samples did not show any evidence for reduced Fe (data not shown).

When ferrihydrite was replaced by hematite in simulated metamorphism experiments, we found that the hematite was less reducible than ferrihydrite. Only 3.3 ± 0.5% of Fe(III) in hematite was reduced if the hematite was mixed with low amounts of dried cells and incubated at 170 °C and 1.2 kbar, while 2.3 ± 0.4% was reduced in mixtures with low amounts of T-pre-treated biomass (Table 1). If the C_{org} content was increased, the Fe(II) yield increased to 11.0 ± 1.1% and 7.0 ± 0.8% in samples with dried and T-pre-treated biomass, respectively (Table 1). Hematite mixed with glucose resulted in similar Fe(II) proportions as samples containing dried cells, with 3.2 ± 0.7% in mixtures with low and 10.9 ± 1.5% in mixtures with high C_{org} (Table 1).

When ferrihydrite was replaced by goethite we observed that the goethite reactivity was intermediate between that of ferrihydrite and hematite when mixed with glucose, with about 15.2 ± 2.1% and 20.7 ± 3.5% of the Fe(III) reduced in the presence of low and high C_{org}, respectively (Table 1). If glucose was substituted by microbial biomass, the Fe(II) yield was higher in goethite samples than in ferrihydrite and hematite samples. In goethite samples with low C_{org} content, the Fe(II) yield was 7.5 ± 0.6% and 6.9 ± 0.9% in samples with dried and T-treated microbial cells, respectively, whereas 17.1 ± 0.5% and 14.8 ± 0.5% Fe(III) was reduced by dried and T-treated microbial biomass, respectively, in samples with high C_{org} content (Table 1).

In samples of biogenic Fe(III) mineral–cell aggregates, 6.2 ± 0.4% and 8.2 ± 0.2% Fe(III) was reduced to Fe(II) and present as siderite in the absence and presence of Si, respectively. This Fe(II) content is comparable to the Fe(II) content measured with synthetic goethite samples with low contents of both dried and T-treated biomass (Table 1).

3.4. Analysis of spatial relationship of different minerals formed by simulated BIF metamorphism

Reflected light microscopy was performed on P/T-treated samples containing initial mixtures of either hematite or ferrihydrite and dried microbial biomass with both low and high C_{org} contents. Although the mineralogy of both samples with initial ferrihydrite or hematite were the same after P/T-incubation as determined by µXRD and Mössbauer spectroscopy (Figs. 2 and 4), the samples with initial ferrihydrite were microscopically clearly distinguishable from the samples that initially contained hematite. The

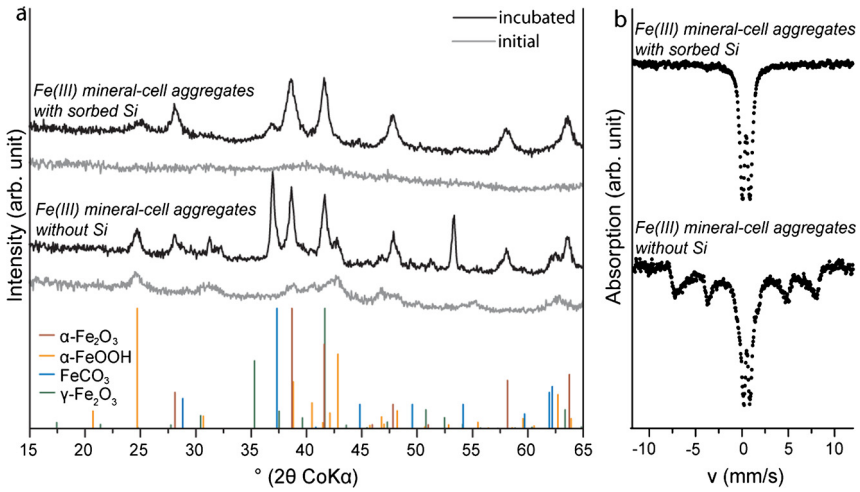

Fig. 3. µXRD analyses of biogenic Fe(III) mineral–cell aggregates from phototrophic Fe(II)-oxidizers grown in the absence and presence of dissolved Si before and after simulated metamorphism (a) and Mössbauer spectra collected at 77 K of biogenic Fe(III) mineral–cell aggregates with and without Si (b).

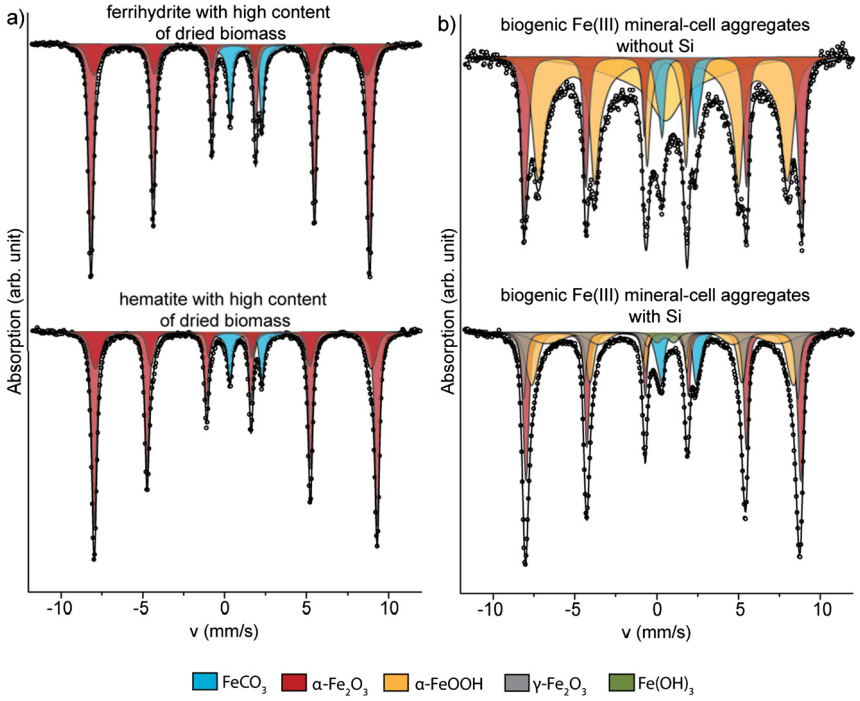

Fig. 4. Mössbauer spectra collected at 140 K of samples of synthetic ferrihydrite and hematite with high content of dried biomass (a) and biogenic Fe(III) mineral–cell aggregates with and without Si (b) after 14 days of simulated metamorphism. Circles: data points, solid black line: fit.

hematite formed from ferrihydrite had a brecciated appearance with irregularly-shaped grains of different sizes (Fig. 5a, c). The surfaces of these grains looked rough with a greyish coloring and red color with crossed polars (Fig. 5a, c). The reddish color came from inner reflections within hematite grains, representing either small hematite grains or hematite grains with many fractures. In samples of initial hematite, hematite was light grey, but appeared almost black where the sample was overlain by resin (Fig. 5b). In contrast to ferrihydrite-derived hematite, the hematite in these samples was black under crossed polars (Fig. 5d), indicating a higher degree of crystallinity and fewer internal fractures. However, areas around hematite were red and represented areas less crystalline in structure (Fig. 5d). Siderite grains were not clearly identified in samples that were formed from initial hematite due to foreign particles (gold, Fig. 5b) or overlying resin (Fig. 5d). In samples that formed from initial ferrihydrite, siderite was visible as light greyish crystals, with and without crossed polars, with a euhedral or subhedral shape (Fig. 5a, c). Siderite crystals were mostly located in pores (Fig. 5a, c) or between single hematite grains.

A combination of XRF and XAS at the Fe K-edge was used to map the Fe oxidation state within a 0.4 × 0.5 mm area of an epoxy-embedded P/T-treated sample initially containing hematite and glucose (high C_{org} content). The analysis showed a matrix of Fe(III) with globules of Fe(II) (Fig. 6b). Based on XRD (Fig. 3b) and Mössbauer spectroscopy results (Table 1), the oxidized areas represent hematite, whereas the reduced areas are siderite. This is consistent with observations by reflected-light microscopy (Fig. 6a). Both size and distribution of siderite crystals are similar in the micrograph and the Fe oxidation state map, showing siderite globules surrounded by hematite (Fig. 6a, b). Furthermore, XANES spectra collected at oxidized and reduced areas in Fig. 6b also confirmed the presence of both hematite and siderite (SI. 16). Although both minerals could be detected in oxidized and reduced areas, the relative abundance of each mineral differed (SI. 16).

Table 1
Fe(II)/Fe(tot) ratios and mineralogy of synthetic Fe(III) mineral–C_{org} mixtures and biogenic Fe(III) mineral–cell aggregates with and without sorbed Si after 14 days of simulated metamorphism determined by Mössbauer spectroscopy.

Fe(III) mineral	C_{org} source	e^--ratio	Fe(II)/Fe(tot) (mol%)	Mineralogy after simulated metamorphism					
				Fe_2O_3	Fe_3O_4	$FeCO_3$	FeOOH	γ-Fe_2O_3	$Fe(OH)_3$
Ferrihydrite	Glucose	0.6	22.8 ± 0.9	x	x	x			
		2.4	43.9 ± 1.6		x	x			
	Dried cells	0.6	4.7 ± 0.6	x		x			
		2.4	14.6 ± 0.3	x		x			
	T-treated cells	0.6	3.2 ± 0.4	x		x			
		2.4	12.0 ± 1.2	x		x			
Hematite	Glucose	0.6	3.2 ± 0.7	x		x			
		2.4	10.9 ± 1.5	x		x			
	Dried cells	0.6	3.3 ± 0.5	x		x			
		2.4	11.0 ± 1.1	x		x			
	T-treated cells	0.6	2.3 ± 0.4	x		x			
		2.4	6.9 ± 0.8	x		x			
Goethite	Glucose	0.6	15.2 ± 2.1		x	x	x		
		2.4	20.7 ± 3.5			x	x		
	Dried cells	0.6	7.5 ± 0.6	x		x	x		
		2.4	17.1 ± 0.5	x		x	x	x	
	T-treated cells	0.6	6.9 ± 0.9	x		x	x		
		2.4	14.8 ± 0.5	x		x	x	x	
Fe(III) mineral–cell aggregates without Si			6.2 ± 0.4	x		x	x		
Fe(III) mineral–cell aggregates with sorbed Si			8.2 ± 0.2	x		x	x	x	x

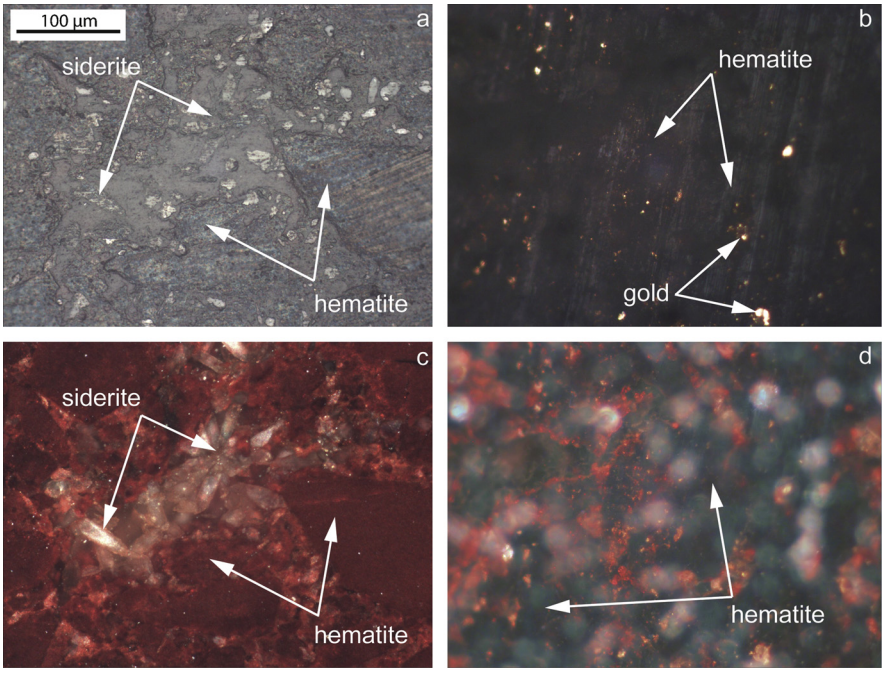

Fig. 5. Reflected-light micrographs of samples after simulated metamorphism initially containing ferrihydrite (a, c) and hematite (b, d) with high C_{org} (dried biomass). Hematite originated from ferrihydrite has heterogeneous grey coloring while siderite is light grey (a). More crystalline hematite usually has a very light grey to whitish color, which appears only weakly in panel b due to overlaying resin. Under crossed polars (c, d) less crystalline hematite appears red and siderite whitish or greyish, whereas more crystalline hematite is black.

4. Discussion

4.1. Thermochemical and microbial formation of magnetite in BIFs – consequences for using magnetite as biomarker

Recently, Posth et al. (2013) suggested thermochemical Fe(III) reduction of primary Fe(III) minerals by glucose as a possible formation pathway of Fe(II)-bearing BIF minerals, such as magnetite. However, in our study, using microbial biomass, we did not observe any magnetite formation after 14 days at 170 °C and 1.2 kbar. A possible reason for the absence of magnetite formation in biomass-containing samples could be that the transformation of Fe(III) oxyhydroxide minerals to magnetite, which requires Fe(II) sorption to the Fe(III) mineral surface followed by solid-state conversion to magnetite (Hansel et al., 2003), is inhibited by adsorption of organic biomolecules leading to surface blocking. For instance, breakdown of the biomass during pressure–temperature treatment of the samples produces some carbohydrates, nucleic acids and proteins (Pistorius et al., 2009; Sanchez-Silva et al., 2012), but also more complex organic molecules, e.g., aromatics (Qin et al., 2008). Furthermore, it has been shown that hydrophobic organic compounds (e.g., aromatics) are preferentially adsorbed to Fe(III) mineral surfaces compared to hydrophilic ones (e.g., glucose; Gu et al., 1995). Thus, in contrast to glucose-containing samples, more complex hydrophobic organic molecules could have been produced in biomass-containing samples during incubation,

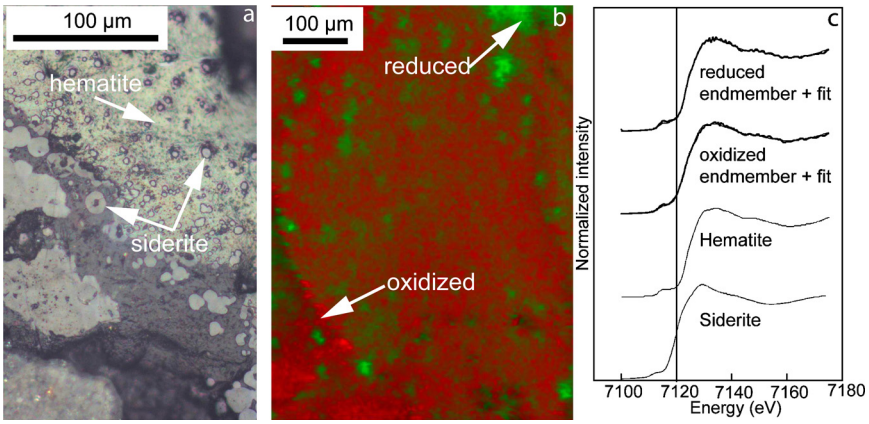

Fig. 6. Reflected-light micrograph (a) and map of Fe oxidation state (b) of a sample initially containing hematite and high content of glucose after simulated metamorphism. Red: Fe(III); green: Fe(II). Two XANES spectra shown are representative for endmembers of oxidized and reduced areas in panel (b) fitted with presented reference spectra of pure hematite and siderite (c). The vertical line represents the energy at 7120 eV.

resulting in higher adsorption and higher degree of mineral surface blocking, preventing magnetite formation. A similar inhibition of magnetite formation by complex organic molecules binding to the surface of Fe(III) oxyhydroxides has been reported for natural environments (Amstaetter et al., 2012).

If magnetite cannot be formed by thermochemical Fe(III) reduction by complex organic materials, then this suggests either that magnetite forms diagenetically via DIR (Lovley et al., 1987; Vargas et al., 1998; Konhauser et al., 2005) or that thermochemical reduction leads to magnetite formation, but only using simple organic substrates (Köhler et al., 2013; Posth et al., 2013). Whether magnetite can be formed with increasing temperatures or with continuing exposure to elevated pressure and/or temperature during metamorphism, which would lead to further degeneration of complex organics and production of simple organic compounds, is still unclear and needs to be tested.

Siderite formation appeared to be independent of the complexity of the organic substrate, likely due to the different mineral formation pathways for siderite and magnetite. While magnetite is formed via a solid state conversion due to interaction of dissolved Fe(II) and Fe(III) (oxyhydr)oxide minerals, siderite is chemically precipitated from a solution containing dissolved Fe(II) and bicarbonate. Thus, as long as dissolved Fe(II) and bicarbonate are present siderite can be formed. Siderite precipitation is in agreement with observations in thin sections of our samples that siderite has euhedral or subhedral shape and that it is located in pore spaces. This suggests that thermochemical Fe(III) reduction during metamorphism can lead to siderite formation. So, what does this mean for interpretations of geochemical signatures in BIF magnetite and siderite? Our results show that DIR-derived magnetite and thermochemical siderite can be precipitated proximal to one another. Assuming Si-coated biogenic ferrihydrite (due to highly concentrated dissolved Si in seawater) as a primary Fe mineral of BIF, it would have been associated with fresh biomass and both would have sedimented simultaneously from the photic zone to the seafloor. During sedimentation, some of the biomass was already degraded by fermentation, but also by anaerobic respiratory processes, such as DIR. In the sediments, during early diagenesis up to temperatures of 120 °C (Kashefi and Lovley, 2000), degradation of biomass by DIR continued, resulting in C_{org} consumption and magnetite formation from the ferrihydrite precursor. With increasing temperature and pressure, residual ferrihydrite was then transformed to hematite, or to goethite given the stabilizing effect of sorbed Si (Toner et al., 2012) as in our experiments with Si-coated biogenic Fe(III) mineral–cell aggregates. Thus, it is reasonable to consider BIF sediments as consisting of goethite (or hematite), magnetite and degraded biomass after early diagenesis. At temperatures above 100 °C, thermochemical Fe(III) reduction of goethite could then produce siderite while diminishing C_{org}. Since Fe(III)-reducing bacteria can only exist at temperatures below 120 °C (Kashefi and Lovley, 2000), while thermochemical Fe(III) reduction probably starts at temperatures higher than 100 °C and still takes place at a few hundred °C (Perry et al., 1973), both processes can occur in the same sediment at different depths, but using different organic substrates. This could lead to different geochemical signatures within DIR-derived and thermochemically produced siderite (e.g., Fe isotope composition; Johnson et al., 2008).

Interestingly, Fe isotope signatures in BIF magnetite and siderite showing heavy and light Fe isotope compositions, respectively, suggest different formation pathways for both minerals (Beard et al., 2003; Johnson et al., 2008). Magnetite is supposed to originate from an abiotic equilibrium reaction of a Fe(III) precursor with dissolved Fe(II) that sorbs to the Fe(III) precipitates (Johnson et al., 2008), whereas isotopically light siderite is proposed as a product of DIR, which leads to a strong Fe isotope fractionating process towards light Fe isotopic compositions of the products (Johnson et al., 2005). However, all these studies do not consider the Fe isotope fractionation by thermochemical Fe(III) reduction during metamorphism, for which the Fe isotope fractionation is completely unknown and which is currently being measured in the authors' laboratory.

4.2. Thermochemical formation and transformation of siderite – information from crystal morphology

Comparison of crystal shapes of thermochemical siderite from our experiments and the study by Köhler et al. (2013) shows that siderite produced by thermochemical Fe(III) reduction in the presence of glucose has globule-like structures (Fig. 6a; Köhler et al., 2013) and, thus appears different to siderite crystals formed from biomass-Fe(III) setups, which have euhedral or subhedral shapes (Fig. 5a, c). Both crystal shapes can be observed in BIF. For example, globule-like siderite was described by Köhler et al. (2013) in samples from the Gunflint Formation in Canada, whereas Ayres (1972) and Beukes et al. (1990) found euhedral siderite grains within kerogen-rich samples from the Dales Gorge Member in the Hamersley Supergroup (Western Australia) and Kuruman Formation of the Transvaal Supergroup (South Africa), respectively. In the case of an initial formation of euhedral siderite by thermochemical Fe(III) reduction during BIF metamorphism, dissolution of the siderite can cause the transformation from euhedral to globule-shaped. Dissolution markers in subhedral siderite grains were also found by Pecoits et al. (2009) in samples from the Dales Gorge

Member, which could be an intermediate between euhedral and globule-like siderite grains.

If the dissolution of siderite crystals is coupled to a redox reaction with hematite, which produces magnetite (Ayres, 1972), then this could potentially explain why globule-shaped siderite and magnetite appear together in samples of ferrihydrite/glucose (both low and high C_{org} content) and goethite/glucose (low C_{org} content). The lack of magnetite formation in hematite samples containing low and high content of glucose, as well as in goethite samples with high glucose content, might be explained by the absence of dehydration (hematite) or lower amount of water released by dehydration (goethite) compared to the release of water during ferrihydrite dehydration. Hematite remained stable during our simulation experiments (Fig. 2, Table 1) and did not dehydrate while goethite is stabilized by C_{org} against transformation (Fig. 2; Table 1) and, thus, dehydration. Therefore, less water was released in goethite samples containing a high content of glucose compared to the goethite samples with the low glucose content. This could have led to a limitation of porewater, and thus a limitation of the Fe(II) transport and diffusion that are required for the solid-state conversion of the Fe(III) (oxyhydr)oxides to magnetite in the absence of complex organic matter. The dependence of magnetite formation on porewater content in glucose-containing samples will be tested in future experiments.

4.3. The contribution of diagenetic (thermochemical) Fe(III) reduction with biomass-C_{org} as reductant to BIF mineralogy

A key question resulting from our data on thermochemical Fe(III) reduction is just how important this process was during BIF sediment burial? Quantification of Fe(II) in all Fe(III) mineral/biomass mixtures tested in this study by Mössbauer spectroscopy revealed that different amounts of Fe(III) were reduced depending on the identity of the starting Fe(III) mineral and on the degeneration state (dried vs. T-treated) of the biomass (Table 1). Generally, in samples containing biomass, hematite was less reactive than ferrihydrite, and goethite showed most Fe(II) formation (except for glucose-containing samples). The fact that ferrihydrite is less reactive than goethite is probably a result of the fast transformation of ferrihydrite to hematite, whereas goethite was not completely transformed due to stabilization of goethite by C_{org}, so that goethite remained partly in its less crystalline and thus more reactive form (Fig. 1) (Jones et al., 2009; Bennett et al., 2014). Differences in reactivity are consequences of differences in crystallinity, surface area and the resulting redox potential (Cornell and Schwertmann, 2003). Any of these factors can lower the thermodynamic driving force for reduction of synthetic hematite and ferrihydrite relative to goethite. In addition, we also observed differences in the extent of Fe(III) reduction by the two types of biomass used. As expected, the T-treated biomass showed a lower reactivity compared to the dried biomass. The T-treatment at 170 °C for 24 hrs degraded a significant fraction of the highly reactive organics, e.g., proteins and polysaccharides (SI. 3; Pistorius et al., 2009; Sanchez-Silva et al., 2012), so that the biomass is depleted in these reactive organic compounds already before mixing with Fe(III) minerals. The lower content of highly reactive compounds led to lower Fe(III) reduction in the simulated metamorphic experiments in samples with T-treated biomass at elevated temperature and pressure. However, the maturity state of the biomass did not affect the final mineralogy.

It is reasonable to assume that Si-coated biogenic ferrihydrite associated with partly degenerated microbial biomass dominated primary BIF sediments. Based on our results using biogenic Si-coated Fe(III) mineral–cell aggregates, goethite was likely the dominant Fe(III) alteration product mineral in BIF sediments with increasing P/T-conditions. However, biogenic Fe(III) mineral–cell aggregates used in our experiments were associated with fresh biomass. Comparable redox characteristics and mineral transformation behavior of synthetic and biogenic goethite allows the usage of the synthetic goethite samples as the most comparable sample with respect to the redox reactivity. Therefore, considering the difference between the reaction time in nature (millions and billions of years) and in our lab experiments (few days), it is reasonable to assume that over the long time span (between 3.8 to 1.9 billion years) the Fe(II) content of 7% revealed here in samples of goethite/T-treated biomass (low content) can increase via thermochemical reduction up to the 60% that is found in representative BIF (Klein and Beukes, 1992). If the C_{org} content in BIF sediments after early diagenesis was higher due to higher input of organic matter (e.g., cyanobacteria present in the upper water column) the Fe(II) yield could be significantly increased.

4.4. Are mixtures of synthetic Fe(III) minerals with biomass representative for the reactivity of biogenic Fe(III) mineral–cell aggregates formed by photoferrotrophs?

Since biogenic Fe(III) minerals have different properties from their abiotic counterparts, specifically crystallinity, surface area, particle size, inclusion of foreign ions, and the association with cells (Konhauser, 1997; Cornell and Schwertmann, 2003; Posth et al., 2010), the comparability of synthetic Fe(III) mineral–C_{org} mixtures was tested using biogenic Fe(III) mineral–cell aggregates produced by the photoferrotrophic strain *R. iodosum*. The biogenic Fe(III) mineral–cell aggregates used consisted of poorly ordered goethite and showed mineral transformations by simulated metamorphism similar to our synthetic goethite/biomass mixtures, i.e., the formation of hematite and siderite plus some remaining goethite (Table 1). Final Fe(II) contents in biogenic and synthetic Fe(III) mineral–C_{org} mixtures after P/T-treatment showed a similar extent of Fe(III) reduction. However, it needs to be considered that the C content in our biogenic aggregates from batch experiments is likely to be higher than in natural aggregates formed in open water columns. In open systems, a significant fraction of the photoferrotrophic cells could have remained planktonic without sedimenting with their Fe(III) mineral products to the seafloor (Posth et al., 2010).

In our experiments, we collected the biogenic Fe(III) mineral–cell aggregates by centrifugation so that our Fe(III) mineral–cell aggregates have an Fe/C ratio corresponding to the ideal stoichiometry of phototrophic Fe(II) oxidation of 4 Fe(III) to 1 CH_2O, i.e., 100% of the microbial cells were in the Fe(III) mineral–cell-aggregates (electron ratio of 1). Consequently, our Fe(III) mineral–cell aggregates contained 40% more C_{org} than natural aggregates and our synthetic mineral/biomass mixtures (with an electron ratio of 0.6). Given the different C_{org} contents in our synthetic mixtures and biogenic Fe(III) mineral–cell aggregates, the Fe(II) yields during thermal treatment of the biogenic Fe(III) mineral–cell aggregates were lower as compared to the synthetic goethite samples and rather similar to synthetic ferrihydrite samples. The lower Fe(II) yield in biogenic Fe(III) mineral–cell aggregates could be caused by different mineral properties of the biogenic goethite compared to the synthetic goethite, such as surface area. Whereas the synthetic goethite had a very small particle sizes (as shown by Mössbauer spectroscopy) and, thus, probably a very high surface area, the goethite particles in the biogenic Fe(III) mineral–cell aggregates could have had larger sizes or less porosity and, so, lower surface area, resulting in less reduction. However, based on the fact that the final mineralogy observed with the synthetic goethite mixtures was similar to the composition of the mineral products obtained with the Fe(III) mineral–cell aggregates, we conclude that our synthetic Fe(III) mineral–biomass mixtures, particularly goethite–

biomass mixtures, can be considered representative of natural biogenic Fe(III) mineral–cell aggregates.

4.5. Influence of silica on thermochemical Fe(III) reduction

In order to consider the high concentration of Si up to 2.2 mM in the Precambrian oceans, we also investigated the P/T-treatment of Fe(III) mineral–cell aggregates with associated Si (Si/Fe ratio of 0.042) produced by *R. iodosum* in the presence of about 1 mM Si. The minerals consisted of ferrihydrite, compared to goethite in the Fe(III) mineral–cell aggregates produced without Si (Fig. 3b). Silica is known to stabilize Fe minerals against transformation to more crystalline phases (Jones et al., 2009; Toner et al., 2012). In our experiments, the interaction of the first Fe(III) polymers forming during microbial Fe(II) oxidation with the Si (Posth et al., 2010) probably prevented the nucleation to more crystalline minerals such as goethite. In addition to the prevention of nucleation, Si also inhibited the transformation of ferrihydrite to hematite during simulated metamorphism as evidenced by the small amount of ferrihydrite even after 14 days of P/T-diagenesis (Fig. 4b). The presence of poorly crystalline ferrihydrite explains the higher Fe(II) yields in P/T-treated biogenic samples with Si compared to setups without Si (Table 1) because it is more reactive with respect to thermochemical Fe(III) reduction than goethite or hematite. Therefore, Si bound to Fe(III) (oxyhydr)oxides in BIF sediments would have influenced the extent of Fe(II) formation, and also the final mineralogy produced by thermochemical Fe(III) reduction.

5. Conclusions

Our study suggests that Fe(III) minerals could have been significantly reduced during metamorphism of BIF sediments as long as C_{org} from microbial biomass was present, resulting in siderite formation. However, solid-state conversion of Fe(III) minerals to magnetite was inhibited by organic compounds from the original microbial biomass. Whether magnetite could be formed thermochemically, over longer timescales or at higher temperatures, with simple organic substrates produced by thermal decomposition of complex organics from microbial biomass as shown in previous experiments (Köhler et al., 2013; Posth et al., 2013) remains to be tested. It is possible that with increasing duration of exposure to elevated temperature and pressure, or with on-going oxidation of C_{org}, the blocked reaction sites of the Fe(III) minerals are unblocked. Consequently, siderite or simple organic compounds could react with the Fe(III) mineral, to ultimately form magnetite. Nevertheless, it is possible that magnetite and siderite located in the same stratigraphic unit in BIF could be of different origins, i.e., thermochemical Fe(III) reduction and DIR, and thus record different geochemical signatures. A possibility which has to be considered in interpretation of the rock record.

Acknowledgements

We would like to thank Christoph Berthold for helping with µXRD measurements, Udo Neumann for his guidance and advices taking reflected-light micrographs, and Sam Webb for his support during measurements at SSRL. This study was supported by the grant KA 1736/24-1 from the German Research Foundation (DFG). KK would like to thank the Natural Sciences and Engineering Research Council of Canada (NSERC) for their financial support (grant 165831).

Appendix A. Supplementary material

Supplementary material related to this article can be found online at http://dx.doi.org/10.1016/j.epsl.2016.06.032.

References

Amstaetter, K., Borch, T., Kappler, A., 2012. Influence of humic acid imposed changes of ferrihydrite aggregation on microbial Fe(III) reduction. Geochim. Cosmochim. Acta 85, 326–341.

Ayres, D.E., 1972. Genesis of iron-bearing minerals in banded iron formation mesobands in the Dales Gorge Member, Hamersley Group, Western Australia. Econ. Geol. 67, 1214–1233.

Beard, B.L., Johnson, C.M., Skulan, J.L., Nealson, K.H., Cox, L., Sun, H., 2003. Application of Fe isotopes to tracing the geochemical and biological cycling of Fe. Chem. Geol. 195, 87–117.

Bekker, A., Slack, J.F., Planavsky, N., Krapež, B., Hofmann, A., Konhauser, K.O., Rouxel, O.J., 2010. Iron formation: the sedimentary product of a complex interplay among mantle, tectonic, oceanic, and biospheric processes. Econ. Geol. 105, 467–508.

Bekker, A., Planavsky, N.J., Krapež, B., Rasmussen, B., Hofmann, A., Slack, J.F., Rouxel, O.J., Konhauser, K.O., 2014. Iron formations: their origins and implications for Ancient Seawater chemistry. In: Turekian, K.K. (Ed.), Treatise on Geochemistry, second edition. Elsevier, Oxford, pp. 561–628.

Bennett, S.A., Toner, B.M., Barco, R., Edwards, K.J., 2014. Carbon adsorption onto Fe oxyhydroxide stalks produced by a lithotrophic iron-oxidizing bacteria. Geobiology 12, 146–156.

Beukes, N.J., Klein, C., Kaufman, A.J., Hayes, J.M., 1990. Carbonate petrography, kerogen distribution, and carbon and oxygen isotope variations in an early Proterozoic transition from limestone to iron-formation deposition, Transvaal Supergroup, South Africa. Econ. Geol., Bull. Soc. Econ. Geol. 85, 663–690.

Braterman, P.S., Cairns-Smith, A.G., Sloper, R.W., 1983. Photo-oxidation of hydrated Fe^{2+}-significance for banded iron formations. Nature 303, 163–164.

Cloud, P.E., 1965. Significance of the Gunflint (Precambrian) microflora: photosynthetic oxygen may have had important local effects before becoming a major atmospheric gas. Science 148, 27–35.

Cornell, R.M., Schwertmann, U., 2003. The Iron Oxides – Structures, Properties, Reactions, Occurrences and Uses. Wiley–VCH Verlag, Weinheim.

Ewers, W.E., Morris, R.C., 1981. Studies of the Dales Gorge member of the Brockman Iron Formation, Western Australia. Econ. Geol. 76, 1929–1953.

Gole, M.J., Klein, C., 1981. Banded iron-formations through much of Precambrian time. J. Geol. 89, 169–183.

Gu, B., Schmitt, J., Chen, Z., Liang, L., McCarthy, J.F., 1995. Adsorption and desorption of different organic matter fractions on iron oxide. Geochim. Cosmochim. Acta 59, 219–229.

Hanesch, M., Stanjek, H., Petersen, N., 2006. Thermomagnetic measurements of soil iron minerals: the role of organic carbon. Geophys. J. Int. 165, 53–61.

Hansel, C.M., Benner, S.G., Neiss, J., Dohnalkova, A., Kukkadapu, R.K., Fendorf, S., 2003. Secondary mineralization pathways induced by dissimilatory iron reduction of ferrihydrite under advective flow. Geochim. Cosmochim. Acta 67, 2977–2992.

Holland, H.D., Lazar, B., McCaffrey, M., 1986. Evolution of the atmosphere and oceans. Nature 320, 27–33.

Holm, N.G., 1989. The $^{13}C^{12}C$ ratios of siderite and organic matter of a modern metalliferous hydrothermal sediment and their implications for banded iron formations. Chem. Geol. 77, 41–45.

Johnson, C.M., Roden, E.E., Welch, S.A., Beard, B.L., 2005. Experimental constraints on Fe isotope fractionation during magnetite and Fe carbonate formation coupled to dissimilatory hydrous ferric oxide reduction. Geochim. Cosmochim. Acta 69, 963–993.

Johnson, C.M., Beard, B.L., Klein, C., Beukes, N.J., Roden, E.E., 2008. Iron isotopes constrain biologic and abiologic processes in banded iron formation genesis. Geochim. Cosmochim. Acta 72, 151–169.

Jones, A.M., Collins, R.N., Rose, J., Waite, T.D., 2009. The effect of silica and natural organic matter on the Fe(II)-catalysed transformation and reactivity of Fe(III) minerals. Geochim. Cosmochim. Acta 73, 4409–4422.

Kappler, A., Newman, D.K., 2004. Formation of Fe(III)-minerals by Fe(II)-oxidizing photoautotrophic bacteria. Geochim. Cosmochim. Acta 68, 1217–1226.

Kappler, A., Pasquero, C., Konhauser, K.O., Newman, D.K., 2005. Deposition of banded iron formations by anoxygenic phototrophic Fe(II)-oxidizing bacteria. Geology 33, 865–868.

Kashefi, K., Lovley, D.R., 2000. Reduction of Fe(III), Mn(IV), and toxic metals at 100 °C by Pyrobaculum islandicum. Appl. Environ. Microbiol. 66, 1050–1056.

Klein, C., Beukes, N., 1992. Time distribution, stratigraphy, and sedimentologic setting, and geochemistry of Precambrian iron-formations. In: The Proterozoic Biosphere: a Multidisciplinary Study, pp. 139–146.

Klein, C., 2005. Some Precambrian banded iron-formations (BIFs) from around the world: their age, geologic setting, mineralogy, metamorphism, geochemistry, and origin. Am. Mineral. 90, 1473–1499.

Köhler, I., Konhauser, K.O., Papineau, D., Bekker, A., Kappler, A., 2013. Biological carbon precursor to diagenetic siderite with spherical structures in iron formations. Nat. Commun. 4, 1741.

Konhauser, K.O., 1997. Bacterial iron biomineralisation in nature. FEMS Microbiol. Rev. 20, 315–326.

Konhauser, K.O., Hamade, T., Raiswell, R., Morris, R.C., Ferris, F.G., Southam, G., Canfield, D.E., 2002. Could bacteria have formed the Precambrian banded iron formations? Geology 30, 1079–1082.

Konhauser, K.O., Newman, D.K., Kappler, A., 2005. The potential significance of microbial Fe(III) reduction during deposition of Precambrian banded iron formations. Geobiology 3, 167–177.

Konhauser, K.O., Amskold, L., Lalonde, S.V., Posth, N.R., Kappler, A., Anbar, A., 2007a. Decoupling photochemical Fe(II) oxidation from shallow-water BIF deposition. Earth Planet. Sci. Lett. 258, 87–100.

Konhauser, K.O., Lalonde, S.V., Amskold, L., Holland, H.D., 2007b. Was there really an Archean phosphate crisis? Science 315, 1234.

Krapež, B., Barley, M.E., Pickard, A.L., 2003. Hydrothermal and resedimented origins of the precursor sediments to banded iron formation: sedimentological evidence from the Early Palaeoproterozoic Brockman Supersequence of Western Australia. Sedimentology 50, 979–1011.

Li, Y.-L., Konhauser, K.O., Cole, D.R., Phelps, T.J., 2011. Mineral ecophysiological data provide growing evidence for microbial activity in banded-iron formations. Geology 39, 707–710.

Li, Y.-L., Konhauser, K.O., Kappler, A., Hao, X.-L., 2013. Experimental low-grade alteration of biogenic magnetite indicates microbial involvement in generation of banded iron formations. Earth Planet. Sci. Lett. 361, 229–237.

Lies, D.P., Hernandez, M.E., Kappler, A., Mielke, R.E., Gralnick, J.A., Newman, D.K., 2005. Shewanella oneidensis MR-1 uses overlapping pathways for iron reduction at a distance and by direct contact under conditions relevant for biofilms. Appl. Environ. Microbiol. 71, 4414–4426.

Lovley, D.R., Stolz, J.F., Nord, G.L., Phillips, E.J., 1987. Anaerobic production of magnetite by a dissimilatory iron-reducing microorganism. Nature 330, 252–254.

Pecoits, E., Gingras, M.K., Barley, M.E., Kappler, A., Posth, N.R., Konhauser, K.O., 2009. Petrography and geochemistry of the Dales Gorge banded iron formation: paragenetic sequence, source and implications for palaeo-ocean chemistry. Precambrian Res. 172, 163–187.

Pecoits, E., Smith, M.L., Catling, D.C., Philippot, P., Kappler, A., Konhauser, K.O., 2015. Atmospheric hydrogen peroxide and Eoarchean iron formations. Geobiology 13, 1–14.

Percak-Dennett, E.M., Beard, B.L., Xu, H., Konishi, H., Johnson, C.M., Roden, E.E., 2011. Iron isotope fractionation during microbial dissimilatory iron oxide reduction in simulated Archaean seawater. Geobiology 9, 205–220.

Perry, E.C., Tan, F.C., Morey, G.B., 1973. Geology and stable isotope geochemistry of the Biwabik iron formation, Northern Minnesota. Econ. Geol. 68, 1110–1125.

Pistorius, A.M.A., DeGrip, W.J., Egorova-Zachernyuk, T.A., 2009. Monitoring of biomass composition from microbiological sources by means of FT-IR spectroscopy. Biotechnol. Bioeng. 103, 123–129.

Posth, N.R., Huelin, S., Konhauser, K.O., Kappler, A., 2010. Size, density and composition of cell–mineral aggregates formed during anoxygenic phototrophic Fe(II) oxidation: impact on modern and ancient environments. Geochim. Cosmochim. Acta 74, 3476–3493.

Posth, N.R., Köhler, I., Swanner, E.D., Schröder, C., Wellmann, E., Binder, B., Konhauser, K.O., Neumann, U., Berthold, C., Nowak, M., Kappler, A., 2013. Simulating Precambrian banded iron formation diagenesis. Chem. Geol. 362, 66–73.

Qin, S., Sun, Y., Tang, Y., 2008. Early hydrocarbon generation of algae and influences of inorganic environments during low temperature simulation. Energy Explor. Exploit. 26, 377–396.

Rasmussen, B., Krapež, B., Meier, D.B., 2014. Replacement origin for hematite in 2.5 Ga banded iron formation: evidence for postdepositional oxidation of iron-bearing minerals. Geol. Soc. Am. Bull. 126, 438–446.

Sanchez-Silva, L., López-González, D., Villaseñor, J., Sánchez, P., Valverde, J.L., 2012. Thermogravimetric–mass spectrometric analysis of lignocellulosic and marine biomass pyrolysis. Bioresour. Technol. 109, 163–172.

Satkoski, A.M., Beukes, N.J., Li, W., Beard, B.L., Johnson, C.M., 2015. A redox-stratified ocean 3.2 billion years ago. Earth Planet. Sci. Lett. 430, 43–53.

Schwertmann, U., Friedl, J., Stanjek, H., 1999. From Fe(III) ions to ferrihydrite and then to hematite. J. Colloid Interface Sci. 209, 215–223.

Schwertmann, U., Cornell, R.M., 2008. Iron Oxides in the Laboratory. John Wiley & Sons.

Siever, R., 1992. The silica cycle in the Precambrian. Geochim. Cosmochim. Acta 56, 3265–3272.

Stookey, L.L., 1970. Ferrozine—a new spectrophotometric reagent for iron. Anal. Chem. 42, 779–781.

Sun, S., Konhauser, K.O., Kappler, A., Li, Y.-L., 2015. Primary hematite in Neoarchean to Paleoproterozoic oceans. Geol. Soc. Am. Bull. 127, 850–861.

Toner, B.M., Berquó, T.S., Michel, F.M., Sorensen, J.V., Templeton, A.S., Edwards, K.J., 2012. Mineralogy of iron microbial mats from loihi seamount. Front. Microbiol. 3, 118.

Vargas, M., Kashefi, K., Blunt-Harris, E.L., Lovley, D.R., 1998. Microbiological evidence for Fe(III) reduction on early Earth. Nature 395, 65–67.

Walker, J.C.G., 1984. Suboxic diagenesis in banded iron formations. Nature 309, 340–342.

Wu, W., Swanner, E.D., Hao, L., Zeitvogel, F., Obst, M., Pan, Y., Kappler, A., 2014. Characterization of the physiology and cell–mineral interactions of the marine anoxygenic phototrophic Fe(II) oxidizer Rhodovulum iodosum—implications for Precambrian Fe(II) oxidation. FEMS Microbiol. Ecol. 88, 503–515.